



# Variability of the extent of the Hadley circulation in the southern hemisphere: a regional perspective

H. Nguyen<sup>1</sup> · H. H. Hendon<sup>1</sup> · E. -P. Lim<sup>1</sup> · G. Boschat<sup>3</sup> · E. Maloney<sup>2</sup> · B. Timbal<sup>1</sup>

Received: 6 December 2016 / Accepted: 17 February 2017 / Published online: 15 March 2017  
© Springer-Verlag Berlin Heidelberg 2017

**Abstract** In order to understand the regional impacts of variations in the extent of the Hadley circulation in the Southern Hemisphere, regional Hadley circulations are defined in three sectors centered on the main tropical heat sources over Africa, Asia-Pacific (Maritime Continent) and the Americas. These regional circulations are defined by computing a streamfunction from the divergent component of the meridional wind. A major finding from this study is that year-to-year variability in the extent of the hemispheric Hadley circulation in the Southern Hemisphere is primarily governed by variations of the extent of the Hadley circulation in the Asia-Pacific sector, especially during austral spring and summer when there is little co-variability with the African sector, and the American sector exhibits an out of phase behavior. An expanded Hadley circulation in the Southern Hemisphere (both hemispherically and in the Asia-Pacific sector) is associated with La Niña conditions and a poleward expansion of the tropical wet zone in the Asia-Pacific sector. While La Niña also promotes expansion in the American and African sectors during austral winter, these tropical conditions tend to promote contraction in the two sectors during austral summer as a result of compensating convergence over the Americas and Africa sectors: a process driven by variations in the Walker

circulation and Rossby wave trains emanating from the tropical Indian Ocean.

## 1 Introduction

The Hadley circulation (HC) refers to the tropical cell of the mean meridional atmospheric circulation and plays an important role in transferring energy and momentum from the tropics to the extra-tropics. The meridional extent and intensity of the downward branch of the HC determine the climate of a large part of the globe, demarking the wet tropics from the dry subtropics. It is well documented that the HC has expanded since the late 1970s (e.g., Seidel et al. 2008; Lucas et al. 2012; Nguyen et al. 2013; Birner et al. 2014). Nguyen et al. (2013) used eight reanalysis datasets to show that the expansion has occurred in most seasons in both the Northern and Southern Hemispheres, but that there has been no significant change in the HC intensity. They also reported that the recent expansion of the Southern Hemisphere (SH) HC has been associated with both the intensification and poleward shift of the subtropical high pressure belt (or subtropical ridge), which especially affect the climate of subtropical Africa, Australia and South America (Nguyen et al. 2015).

Although the HC averaged over the hemisphere has clearly been expanding since 1979, the link between HC expansion and regional changes in climate has remained elusive due in part to the difficulty in computing regional indices of the HC. By nature of the computation using the Stokes streamfunction and in order to conserve the mass flux in the zonal direction, the HC has traditionally been defined from a hemispheric perspective. Thus, quantifying variations of the HC regionally remains an ongoing research question.

✉ H. Nguyen  
hanh.nguyen@bom.gov.au

<sup>1</sup> Bureau of Meteorology, Melbourne, Australia

<sup>2</sup> Department of Atmospheric Science, Colorado State University, Fort Collins, CO, USA

<sup>3</sup> ARC Centre of Excellence for Climate System Science and School of Earth Sciences, University of Melbourne, Melbourne, Australia

Lucas et al. (2012) and Lucas and Nguyen (2015) used radiosonde data as a measure of the edge of the tropics. Those radiosonde measurements are limited to the land only, therefore regional tropical edges were defined over the three continental sectors, and the average over the three continental sectors is assimilated to the hemispheric tropical edge. Their findings based on annual mean since 1979, show tropical expansion in both hemispheres but with marked hemispheric and regional variability. In particular the Australia-New Zealand (ANZ) sector exhibited the largest expansion with significant correlation relationship with the Pacific decadal oscillation (PDO) and Southern annular mode (SAM). Further, Lucas et al. (2012) and Lucas and Nguyen (2015) compared these radiosonde based tropical edge measurements with four reanalysis products, including the ERA-Interim reanalysis. The results suggest that while interannual variability was well captured in all reanalysis products, long-term trends depended on the reanalysis used. This discrepancy was attributed to the tropopause algorithm and the relatively coarse vertical resolution of the reanalyses.

Recently, Chen et al. (2014) defined six regional HCs based on the location of the upward motion in the different climate regions. They used the vertical shear of the divergent meridional wind in the lower and upper troposphere to estimate the regional HC intensity (following Moore et al. 2004) and a threshold for outgoing longwave radiation (OLR) to estimate the HC edge (following Hu et al. 2011). However, estimations of the HC edge using OLR are dependent on the threshold applied, suggesting that OLR is overall inadequate for estimating HC properties (Davis and Rosenlof 2012; Lucas et al. 2013).

Schwendike et al. (2014) decomposed the overturning divergent circulation into the meridional (Hadley) and zonal (Walker) components. In this study, the overturning streamfunction for the HC is derived from the divergent meridional wind and the overturning streamfunction for the Walker circulation was derived from the divergent zonal wind. Their approach allows for the determination of local (limited domain) overturning circulations, with the hemispheric HC recovered by averaging across all locally defined circulations. They further showed that in general the mass flux (overturning) in the local HC is about an order of magnitude larger than in the Walker circulation, thereby supporting the utility of assessing variations of the HC locally.

In this study we adopt the approach of Schwendike et al. (2014) to define the local HC and investigate further interannual variations of the regional HCs. We particularly focus on variations in the poleward edge of the regional HCs in the SH, including the seasonality, inter-relationships between regions and with the hemispheric mean behavior, and associations with key modes of climate variability.

The data and method used to diagnose the HC regionally are presented in Sect. 2. The climatology and interannual variability of the regional HCs are described in Sect. 3. Sections 4 and 5 explore the relationships of the regional HCs with the global HC variations, with tropical sea surface temperatures, and with the main modes of climate variability in the SH including ENSO and the SAM. Discussion and concluding remarks are provided in Sect. 6.

## 2 Data and methods

Reanalysis and observational datasets are used in this study. The reanalysis dataset is the ERA-Interim (ERA1) from the ECMWF (Dee et al. 2011), available from 1979 to present with a spatial resolution of  $0.75^\circ \times 0.75^\circ$ . The observational global rainfall dataset is version 2.2 from the Global Precipitation Climatology Project (GPCP; Huffman et al. 2009). The GPCP analyses are derived from in situ rain gauge measurements combined with satellite estimates and have a horizontal resolution of  $1^\circ \times 1^\circ$  and cover the period 1979 through to present. The SST analyses used in the study are the Version 1.1 of the Hadley Centre Sea Ice and Sea Surface Temperature (HadISST) from the Met Office Hadley Centre (Rayner et al. 2003). HadISST spans from 1870 to present and has a horizontal resolution of  $1^\circ \times 1^\circ$ .

We will explore the relationship between variations of HC edges and some key modes of climate variability. For ENSO, we use the Nino3.4 SST index (average SST anomalies over  $5^\circ\text{N}$ – $5^\circ\text{S}$ ,  $170$ – $120^\circ\text{W}$ ). For variability of the Indian Ocean Dipole, we use the Dipole Mode Index (Saji et al. 1999), which is formed by the difference of SST in the western ( $10^\circ\text{N}$ – $10^\circ\text{S}$ ,  $50^\circ\text{E}$ – $70^\circ\text{E}$ ) and eastern Indian Ocean ( $\text{Eq}$ – $10^\circ\text{S}$ ,  $90^\circ\text{E}$ – $110^\circ\text{E}$ ). We will also explore variability related to north–south shifts of the SH eddy-driven jet as captured by the SAM index and given by the first EOF of the 700 hPa geopotential height (Thompson and Wallace 2000). High SAM values indicate a poleward shift of the eddy-driven (subpolar) jet and have previously been related to a poleward expansion of the HC during austral summer (e.g. Kang and Polvani 2011; Hendon et al. 2014).

All the data used for the study are monthly means for the common period 1979–2014. In order to focus on interannual behavior, the data were detrended prior to computing correlation or regression coefficients. Statistical significance is tested with the Pearson's  $r$  test using the null hypothesis of no relationship.

The HC is unambiguously defined for axisymmetric (zonal mean) two-dimensional flow. In this case, mass conservation in spherical coordinates:

$$\frac{\partial[\rho v \sin y]}{\partial y} + \frac{\partial[\rho \omega]}{\partial p} = 0,$$

where  $v$  is the meridional velocity and  $\omega$  is the pressure vertical velocity and brackets are zonal mean, allows for the flow to be fully defined by the Stokes streamfunction  $\Psi$ :

$$[v] = \frac{1}{a \cos y} \frac{\partial \Psi}{\partial p} \text{ and } [\omega] = \frac{1}{a \cos y} \frac{\partial [\Psi \cos y]}{\partial y}$$

The streamfunction  $\Psi$  is derived as:

$$\Psi(p, y) = \frac{2\pi a \cos y}{g} \int_0^p [v(p, y)] dp \quad (1)$$

where  $a$  is the radius of Earth and  $g$  is the gravitational acceleration.

Following the approach of Schwendike et al. (2014), which states that the atmospheric vertical motion in pressure coordinates can be decomposed into a zonal and a meridional overturning motion, we derive a local meridional overturning streamfunction to depict the local HC. This is done by decomposing the winds into rotational  $\overline{V}_r$  and divergent  $\overline{V}_d$  components in spherical coordinates, noting that only the latter contributes to the vertical motion. The divergent component of the meridional flow can be regarded as the meridional overturning circulation (i.e. the HC) and the divergent component of the zonal flow as the zonal overturning circulation (i.e. the Walker circulation). Mass continuity for the divergent circulation is satisfied independently in the zonal and meridional directions because the two circulations are in orthogonal planes, so that the meridional overturning circulation (the HC) can be represented by a streamfunction derived from the divergent meridional wind similar to Eq. (1):

$$\Psi_d(y, p) = \frac{2\pi a \cos y}{g} \int_0^p [v_d(y, p)] dp \quad (2)$$

Brackets in this case refer to a zonal average over a specified limited (or hemispheric) domain. The divergent

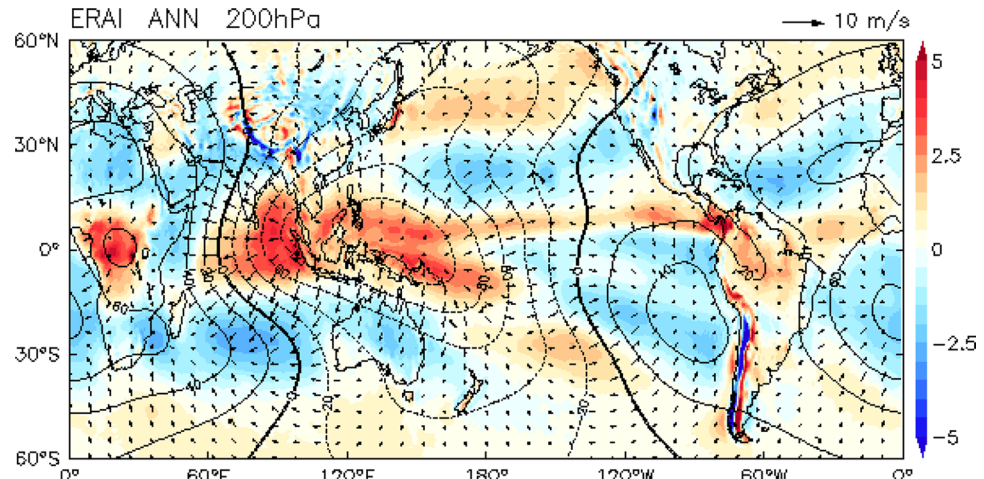
meridional wind  $v_d$  is obtained from the velocity potential that is derived from the total zonal and meridional winds. Note that the Walker circulation which is the zonal component of the total vertical motion, can be represented in a similar way by a zonal streamfunction derived from the divergent zonal wind  $u_d$  along the equator:

$$\Psi_d(x, p) = \frac{2\pi a}{g} \int_0^p [u_d(x, p)] dp \quad (3)$$

This method (i.e., Schwendike et al. 2014) assures the decomposition of the divergent motion into two unique orthogonal overturning circulations that are the sum of the total divergent flow.

The annual mean climatology of the divergent wind fields and velocity potential in the upper troposphere (200 hPa) from the ERAI reanalysis are displayed in Fig. 1. Three main centers of divergence along the equator are clearly seen, depicting the upward branch of the HC over South Africa, South America and over the Maritime Continent and Indo-Pacific tropical warm pool. The corresponding convergence zones, primarily associated with meridional convergence (e.g., Schwendike et al. 2014), are seen in the subtropics flanking these three regions of divergence. In order to quantify regional variations in the HC, we define three (unequal) sectors that are centered on the three regions of divergence: the Asia-Pacific sector ( $AP=65^\circ E-140^\circ W$ ), the Europe-Africa sector ( $EA=20^\circ W-65^\circ E$ ) and the sector of the North and South Americas ( $AA=140^\circ W-20^\circ W$ ). We verified that modest variations in the longitudinal boundaries do not modify our main results. As our focus is the SH, we will also sometimes refer to these EA, AP and AA regions as the African ( $HC_{Afr}$ ), Australian ( $HC_{Aus}$ ) and South American ( $HC_{SA}$ ) cells, respectively. The annual mean meridional (Hadley) streamfunctions for these three regions are shown in Fig. 2. By construction, the sum of the streamfunctions from the

**Fig. 1** Annual mean climatology of the divergent winds (arrows,  $m s^{-1}$ ), divergence (shading,  $s^{-1}$ ) and velocity potential (contours,  $10^{-5} s^{-2}$ ) at 200 hPa from the ERAI reanalysis, for 1979–2010



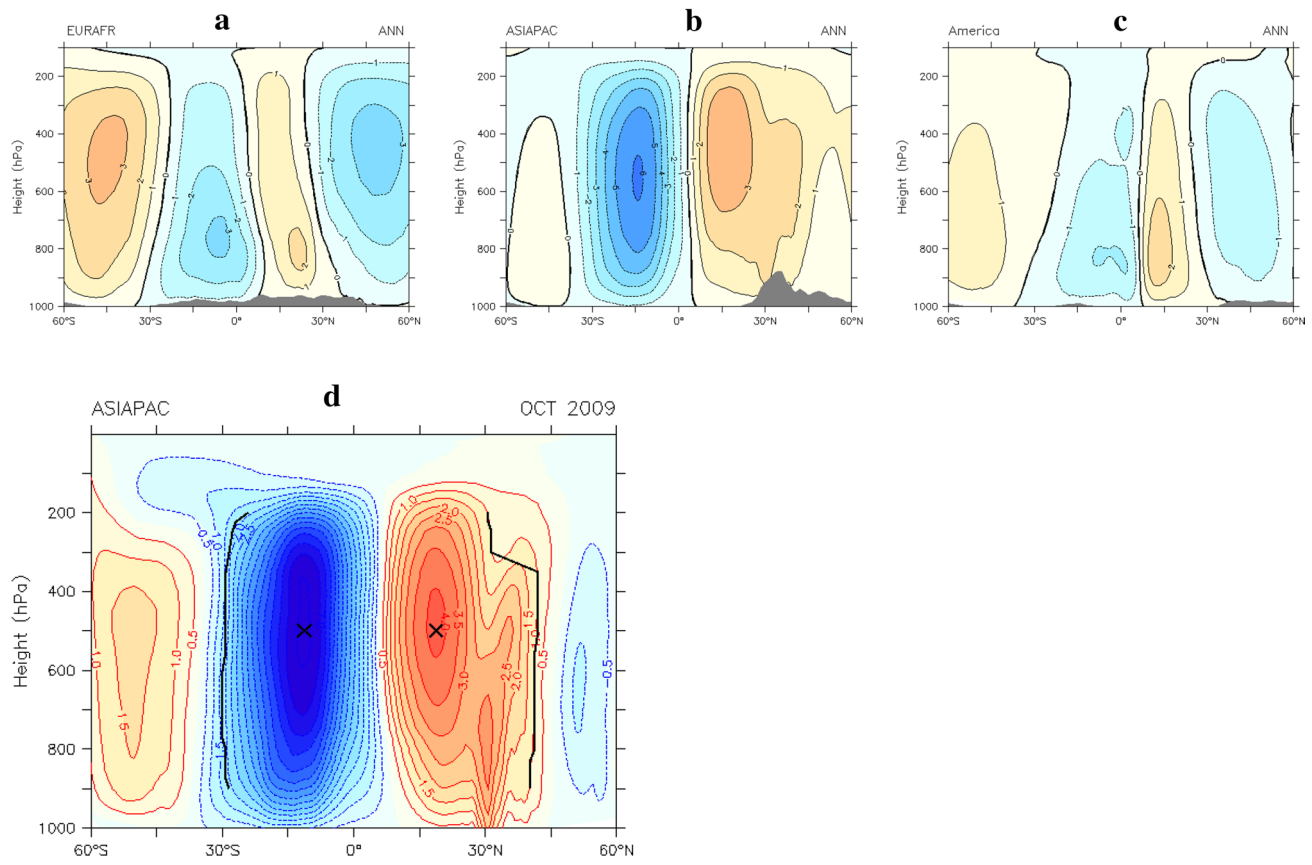


**Fig. 2** (top) Annual mean climatology of the mass streamfunction ( $10^9 \text{ kg s}^{-1}$ ) derived from the divergent wind fields for **a** Europe-Africa, **b** Asia-Pacific and **c** Americas from the ERAI reanalysis. (bottom) Asia-Pacific zonal mean monthly meridional streamfunction

from the ERAI reanalysis with overturning cell peaks indicated by the *black crosses* and edges defined as when the streamfunction values first reach 25% of the peak value indicated by the *vertical black lines* for each pressure level of the troposphere (900–200 hPa)

three regions is equal to the streamfunction derived from the zonal mean meridional velocity.

Our next step is to derive the poleward edge of the HC in each sector. The mean circulation in each sector (Fig. 2) illustrates some potential difficulty to define the poleward edges. In all three sectors equatorial symmetric HC are clear (because we are showing annual mean conditions). However, this regional view highlights that the regional HC is much stronger and deeper in the Asia-Pacific sector but it is not clearly bound in the subtropics by Ferrel cells as in the other two sectors. Hence, although the edge of the zonal mean (hemispheric) HC is commonly characterized as the poleward extent of the descending branch and defined as the location where the streamfunction goes to zero (e.g., Oort and Yienger 1996), the streamfunction for the regional cell does not necessarily reach a zero value at its poleward edge (e.g., the NH cell in Fig. 2b). As a result, we define the edge of the regional HC as where the streamfunction reduces to a specified percentage of the maximum streamfunction value in the tropics. Thresholds of 10, 15, 20 and 25% were tested and results were compared to the zero

value from the hemispheric cells. The results (not shown) indicate that although the mean HC edge was sensitive to the choice of threshold, the year to year variability was not (correlation coefficients exceeding 0.9). Since a higher value ensures a more robust detection of the edge of the HC without impacting its variability, the 25% threshold is used. The edge of the HC is therefore defined as the averaged position of the 25%-peak value between 700–400 hPa. This definition is illustrated in Fig. 2d for a typical case.

### 3 Climatology and variability of the regional Hadley circulations

Using the method described in Sect. 2, we define the poleward extent of the HC in each sector for every month of 1979–2014. The mean seasonal cycle of the latitude of the HC extent or edge (HE) in the SH for the hemispheric ( $\text{HE}_{\text{SH}}$ ) and regional HCs ( $\text{HE}_{\text{Afr}}$ ,  $\text{HE}_{\text{Aus}}$  and  $\text{HE}_{\text{SA}}$ ) is shown in Fig. 3a. The seasonal evolution of extent of the  $\text{HE}_{\text{SH}}$  displays expected behavior: the HC extends farthest

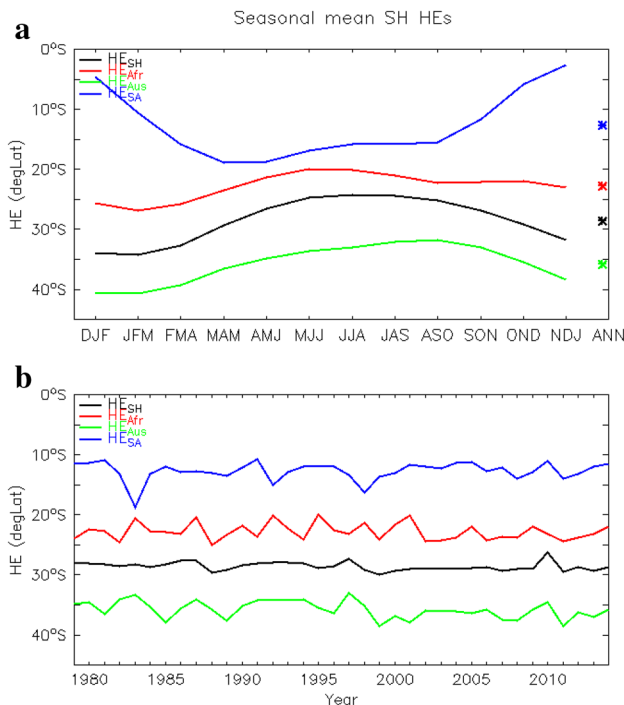


**Fig. 3** **a** Seasonal cycle and **b** annual mean variation of the hemispheric ( $HE_{SH}$ ) and three regional Hadley cell edges ( $HE_{Afr}$ ,  $HE_{Aus}$  and  $HE_{SA}$ ) in the Southern Hemisphere from the ERAI reanalysis. The asterisks on the right of **a** represent the annual mean HEs

into the SH during summer (DJF) and is most confined to the equator during winter (JJA). The seasonal evolutions of  $HE_{Afr}$  and  $HE_{Aus}$  follow a similar cycle, but with  $HE_{Aus}$  greater and  $HE_{Afr}$  less than  $HE_{SH}$ . In contrast,  $HE_{SA}$ , which is the closest to the equator in the mean, shows the opposite seasonal cycle to  $HE_{Afr}$  and  $HE_{Aus}$  (i.e. closest to the equator in summer and farthest in winter). Although the overturning circulation over the American sector is often too weak in summer to accurately define, this out-of-phase seasonal behavior with the other two sectors and with the hemispheric mean may also reflect a primary role for zonal convergence in the region associated with the Pacific Walker Circulation (e.g. Schwendike et al. 2014), such that when the upward branch of the HC is strongest and most poleward in the Asian-Pacific sector during summer, the corresponding convergent branch of the Walker circulation is also strongest in the American sector.

In order to understand the interannual variability of the edges of the three regional HCs and their relationship with the variability of the  $HE_{SH}$ , we display the time series of annual mean HEs in Fig. 3 and the correlation of  $HE_{SH}$  with the extent in the other regions in Fig. 4. A key finding from Fig. 3b is that the interannual variability of annual mean  $HE_{Aus}$  closely follows  $HE_{SH}$  (correlation coefficient is 0.66; indicated by asterisk on right ordinate in Fig. 3). Although variability of annual mean  $HE_{Afr}$  and  $HE_{SA}$  is as

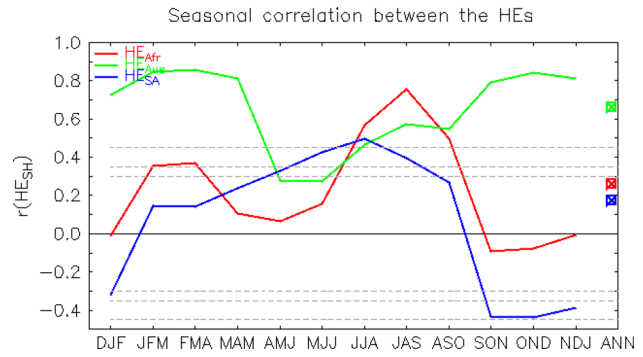


**Fig. 4** Correlation of annual (asterisks) and seasonal (curves) mean  $HE_{SH}$  with regional HEs over three domains (Africa, Australia and South America). The  $r$  test 90, 95, 99% levels are indicated by the horizontal grey dashed lines. Data are from ERAI

large as that of  $HE_{Aus}$  it is not coherent with  $HE_{SH}$  (correlation coefficient is 0.26 and 0.17, respectively; indicated as asterisks on right ordinate in Fig. 4). The large variability in these two cells might reflect uncertainty in detecting the extent in these much weaker circulations. However, at face value this result suggests that it is potentially meaningless to infer regional impacts in the African and American sectors from hemispheric variations of HC extent because the hemispheric variability is dominated by the behavior in the Asia-Pacific sector and is incoherent with the variability in the other two sectors.

The seasonal cycle of the covariation of the HE in each sector with the extent of the hemispheric cell is also displayed in Fig. 4. The variation of  $HE_{Aus}$  is positively correlated with that of  $HE_{SH}$  year round, but the correlation is strongest in the non-winter months. Conversely,  $HE_{Afr}$  is significantly positively correlated with  $HE_{SH}$  only during the winter months.  $HE_{SA}$  is also positively correlated with  $HE_{SH}$  in the winter months but is distinctly anti-correlated with  $HE_{SH}$  during the summer months. These results are consistent with the notion that summertime expansion of  $HE_{Aus}$  is accompanied by changes in the Walker circulation, which act to contract the HC in the South America region (Schwendike et al. 2014).

#### 4 Relationship between Hadley circulation extent and modes of climate variability

Computation of the HC in regional sectors provides an opportunity to better capture how dominant modes of climate variability drive interannual variability of the HC. Correlation coefficients between the extent of the three regional HCs and indices of modes of variability that are known to affect the extent of the HC, such as ENSO (Nino3.4), the IOD (DMI), and the SAM, are analyzed. The

first two indices (Nino3.4 and DMI) reflect variability of the tropical Indo-Pacific SST, which have previously been associated with north–south shifts of the HC arising from variations in tropical convection (e.g. Ashok et al. 2007; Lu et al. 2008). The SAM index captures north–south shifts of the extratropical eddy-driven jet, which has been shown to be related to variations of HE<sub>SH</sub> primarily during the summer months (Kang and Polvani 2011; Hendon et al. 2014). These correlation coefficients are computed for annual mean and seasonally in 3-month windows (Fig. 5).

The Nino3.4 index is negatively correlated with HE<sub>SH</sub> in all seasons (Fig. 5a), but the correlation is weak in autumn (MAM) and strongest in late spring (OND). This confirms that an expanded HC is associated with La Niña-like

conditions throughout the year (e.g., Lu et al. 2008) but less so in autumn, which is the low point in the annual cycle of ENSO. The correlation of Nino3.4 with HE<sub>Aus</sub> follows a similar seasonal cycle but the magnitude of the anti-correlation is generally stronger as compared with HE<sub>SH</sub> and the minimum anti-correlation is shifted to winter. The stronger anti-correlation for HE<sub>Aus</sub> as compared to HE<sub>SH</sub> seems reasonable since ENSO anomalies in convection are strongest in the Australian sector. In contrast to the correlation of HE<sub>Aus</sub>, HE<sub>SA</sub> and HE<sub>Afr</sub> show distinctly maximum negative correlation with Nino3.4 only during winter but positive correlation during spring and early summer. Again, this opposite relationship of HE<sub>Afr</sub> and HE<sub>SA</sub> with Nino3.4 compared to HE<sub>Aus</sub> during summer suggests a role of the Walker circulation such that when La Niña (El Niño) acts during summer months to promote expansion (contraction) in the Australian sector, compensating contraction (expansion) occurs in the South American and African sectors. The more consistent negative correlation of all three sectors with Nino3.4 during winter occurs when the impact of ENSO on the Australian sector is the weakest.

The correlation with the DMI is shown in Fig. 5b. The correlations are only significant during austral spring, which is the season of maximum amplitude of the IOD (e.g. Zhao and Hendon 2009). IOD events also tend to co-occur with ENSO: positive IOD, when eastern Indian Ocean SST is below normal, tends to occur in conjunction with El Niño conditions in the Pacific during spring ( $r(\text{Nino3.4}, \text{DMI}) \sim 0.7$  for the period post 1979 - see also; e.g. Cai et al. 2011). During the spring months when the IOD is most active, the correlation of HE<sub>SH</sub> and HE<sub>Aus</sub> with the DMI is negative, consistent with their negative correlation with Nino3.4. And, the correlation of HE<sub>SA</sub> and HE<sub>Afr</sub> is positive, also consistent with the positive correlation with Nino3.4. These positive correlations are stronger than those computed with Nino3.4, suggesting that SST variations in the Indian Ocean region are a more primary driver of the variation of the Walker Circulation that acts to remotely connect the Hadley circulation response over the Australian sector with that over Africa and South America.

The correlations of the HEs with the SAM index are not as strong as the relationships with the ENSO index (Fig. 5c). However, the previously detected co-variation of HE<sub>SH</sub> with the SAM during summer and lack of relationship during winter (e.g. Kang and Polvani 2011; Hendon et al. 2014) is observed. A similar but stronger annual variation of correlation is observed for HE<sub>Aus</sub>. The relationship with the SAM in the other two sectors is always weak and non-significant. The co-variation of high SAM with HE<sub>SH</sub> and HE<sub>Aus</sub>, during spring/summer is attributable to the eddy-mean flow feedback (e.g. Chen and Held 2007; Kang and Polvani 2011; Hendon et al. 2014). The linkage of SAM with HE<sub>SH</sub> and HE<sub>Aus</sub>, during these warm seasons can

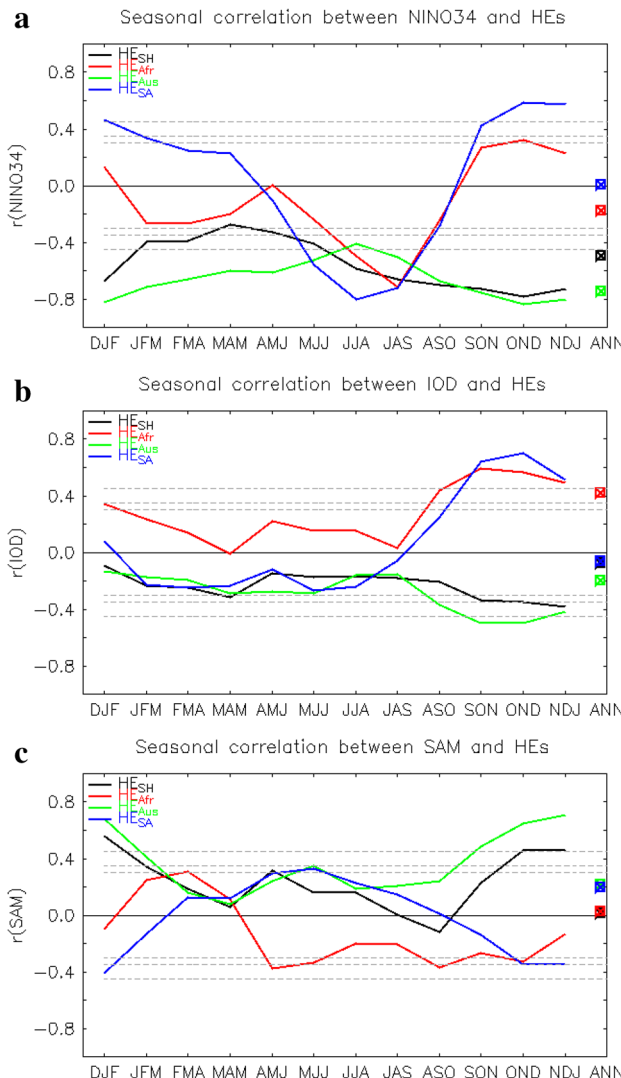


**Fig. 5** Correlation of the annual and seasonal mean HE<sub>SH</sub>, HE<sub>Aus</sub>, HE<sub>Afr</sub>, HE<sub>SA</sub> and **a** the NINO3.4 index, **b** DMI index and **c** SAM index. The  $r$  test 90, 95, 99% levels are indicated by the horizontal grey dashed lines

also be promoted by ENSO (e.g. L'Heureux and Thompson 2006; Lu et al. 2008; Lim and Hendon 2015). Overall, these correlation coefficients summarize the co-variation of tropical and extra-tropical modes with expansion/contraction of the HC (hemispherically and in each sector). The strongest relationships are in spring to early summer: an expanded HC hemispherically and in the Australian sector is associated with La Niña-like conditions, negative IOD and high SAM. It is noteworthy that these same conditions lead to a contraction of the HC in the South American and African sectors. This highlights the interplay between the zonal Walker circulation and the meridional Hadley circulation (e.g. Schwendike et al. 2014).

## 5 Circulation anomalies associated with the Hadley circulation

In order to provide insight into the causes and inter-relationship of the variations in the hemispheric and regional HCs, we compute regressions of rainfall, SST and circulation onto the standardized HE indices. First, annual mean regressions onto the hemispheric  $HE_{SH}$  are analyzed. Second, winter and spring regressions based on regional HEs are presented to highlight the regional and seasonal characteristics of the circulation associated with variations of the HC.

### 5.1 Annual mean regression onto hemispheric Hadley cell

Figure 6 shows the regression of annual mean 200 hPa divergence, velocity potential (VP) and divergent winds onto the time series of normalized annual mean  $HE_{SH}$ . An expanded  $HE_{SH}$  is associated with a clear zonal dipole

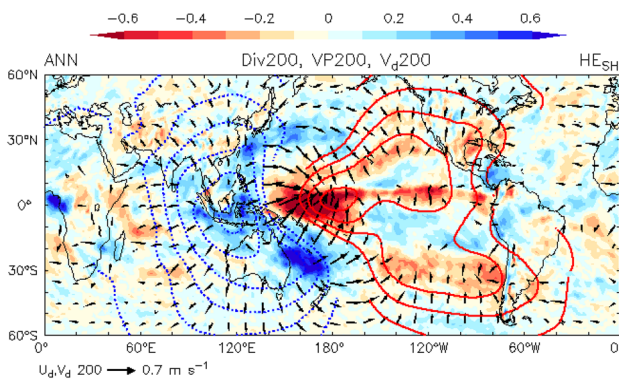


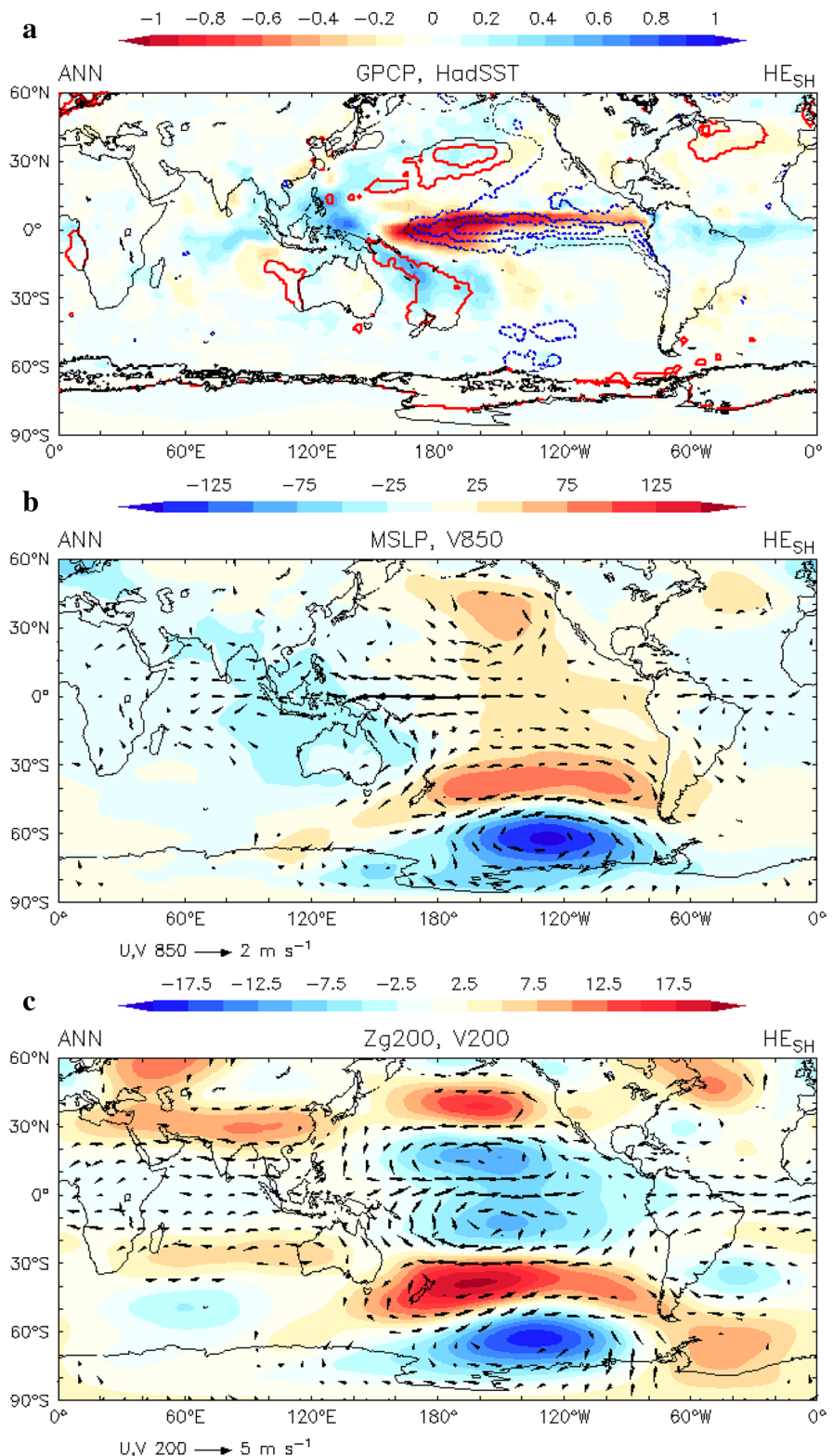
**Fig. 6** ERAI detrended annual mean divergence (shading,  $10^{-6} \text{ s}^{-1}$ ), velocity potential (contours,  $10^5 \text{ m}^2 \text{ s}^{-1}$ ) and divergent winds (arrows,  $\text{m s}^{-1}$ ) at 200 hPa regressed onto standardized  $HE_{SH}$  index. Only vector and contour values statistically significant at the 90% level are shown

of VP, with divergence over the Maritime Continent and convergence over the tropical central and eastern Pacific Ocean. Compared with climatology (Fig. 1), the region of negative VP over the Maritime Continent coincides with the strongest mean center of action, while the other two centers (Africa and South America) show more limited change. This regression confirms that a hemispherically expanded HC is associated with an anomalous Walker circulation, with enhanced divergence over the Maritime Continent/Australian region and enhanced convergence (contraction) in the eastern Pacific.

Figure 7 shows the regression of annual mean rainfall, SST, MSLP, 850 hPa winds and 200 hPa geopotential height and winds onto the standardized  $HE_{SH}$ . These regressions show that a hemispherically expanded HC is associated with a La Niña-like state in the tropical Pacific and a positive Southern Oscillation (lower surface pressure in the Australian sector and higher surface pressure in the equatorial eastern Pacific). The regressed rainfall and SST patterns are characterized by cold SST in the eastern equatorial Pacific and warm in the west, enhanced rainfall over the tropical eastern Indian Ocean and Maritime Continent extending southward into the South Pacific Convergence Zone (SPCZ) to the east of Australia, and reduced rainfall in the eastern Pacific (Fig. 7a). Pacific-South American (PSA) and Pacific North American (PNA) equivalent barotropic wave train patterns are seen extending into the extratropics of the Southern and Northern Hemispheres over the Pacific, respectively (Fig. 7b,c). These regressions emphasize that a hemispherically expanded HC can be viewed as a result of a Gill (1980) response to enhanced tropical heating in the Indian Ocean-Maritime Continent region, which has baroclinic structure in the vertical (circulation anomalies of opposite sign in the upper troposphere, Fig. 7b, c). Necessarily then, an expanded hemispheric HC results in a regional contraction in the western Hemisphere and a more pronounced expansion in the Australian sector.

To briefly summarize the seasonality of the relationship of  $HE_{SH}$  with the large scale circulations based on the correlation coefficients shown in Fig. 5 and regression of the seasonal mean variables in the same way as for the annual mean shown in Fig. 7 (not shown in the paper), an expanded hemispheric HC is associated with La Niña-like conditions in all seasons (Fig. 5a). On the other hand, the PSA/PNA wave trains emanating into the extratropics from the tropical Pacific in relation to the expansion of the  $HE_{SH}$  are most prominent into the respective winter hemispheres as the region of anomalous divergence in the Australian sector tends to shift into the winter hemisphere. A strong high SAM response (circumpolar band of low pressure in the polar region and high pressure equatorward of  $60^\circ\text{S}$ ) is found in summer, being consistent with the correlations shown in Fig. 5.

**Fig. 7** Detrended annual mean variables regressed onto standardized HE<sub>SH</sub> index. **a** GPCP rainfall (shading every 0.1 mm day<sup>-1</sup> with blue colors indicating wet anomalies) and HadSST (contour every 0.1 K with red contours indicating warm anomalies, black contours are not statistically significant at the 90% level). **b** ERAI MSLP (shading every 25 Pa) and 850 hPa horizontal wind (vectors, m s<sup>-1</sup>). **c** 200 hPa ERAI geopotential height (Zg; shading 10 m) and horizontal wind (vectors, m s<sup>-1</sup>). Only the wind vector values statistically significant at the 90% level are shown



## 5.2 Seasonal mean regression onto regional Hadley cells

To further understand regional variability of the HC, we

explore the regressions onto the regional HEs. Based on the seasonality of the relationships between the regional and hemispheric HEs shown in Fig. 4, we concentrate on the regressions during winter (JJA) when all three

regional HEs are positively correlated with the hemispheric HE and during spring (SON) when the correlations between  $HE_{SH}$  and  $HE_{SA}$  and  $HE_{Afr}$  are negative but the correlation for  $HE_{Aus}$  remains positive. The regressions for JJA and SON are shown in Fig. 8 for 200 hPa divergence, VP and divergent winds, in Fig. 9 for rainfall and SST, in Fig. 10 for MSLP and 850 hPa winds and heights, and in Fig. 11 for 200 hPa winds and heights. In each figure, the regressions are onto  $HE_{Aus}$ ,  $HE_{SA}$  and  $HE_{Afr}$  (top to bottom) and during JJA and SON (left to right).

During both seasons, the regressed patterns of divergence, VP and divergent winds onto  $HE_{Aus}$  (Fig. 8a, b) are similar to the regression onto the hemispheric  $HE_{SH}$  (consistent with the positive correlation between the two HE indices shown in Fig. 3). In winter the divergence, VP and divergent wind anomalies regressed onto  $HE_{SA}$  and  $HE_{Afr}$  contribute to further increase and spatially broaden the

anomalies regressed onto  $HE_{Aus}$ , but in spring the patterns are distinctly opposite to that regressed onto  $HE_{Aus}$ .

The regressed SST and rainfall anomalies (Fig. 9) show that in winter all three regional HEs are related to La Niña conditions, although the association for  $HE_{SA}$  is weak and is more characteristic of La Niña Modoki (Ashok et al. 2007), which is also referred to as central Pacific La Niña (Kao and Yu 2009). During spring, an expanded HE in the Australian sector is still associated with La Niña conditions in the Pacific and negative IOD conditions in the Indian Ocean, but an expanded  $HE_{SA}$  and  $HE_{Afr}$  is now associated with El Niño and positive IOD conditions. Therefore, during spring (and summer, not shown) La Niña drives expansion hemispherically and in the Australian sector, but it drives contraction in the South American and African sectors.

The low-level (Fig. 10) and upper tropospheric (Fig. 11) circulation anomalies confirm that an expanded

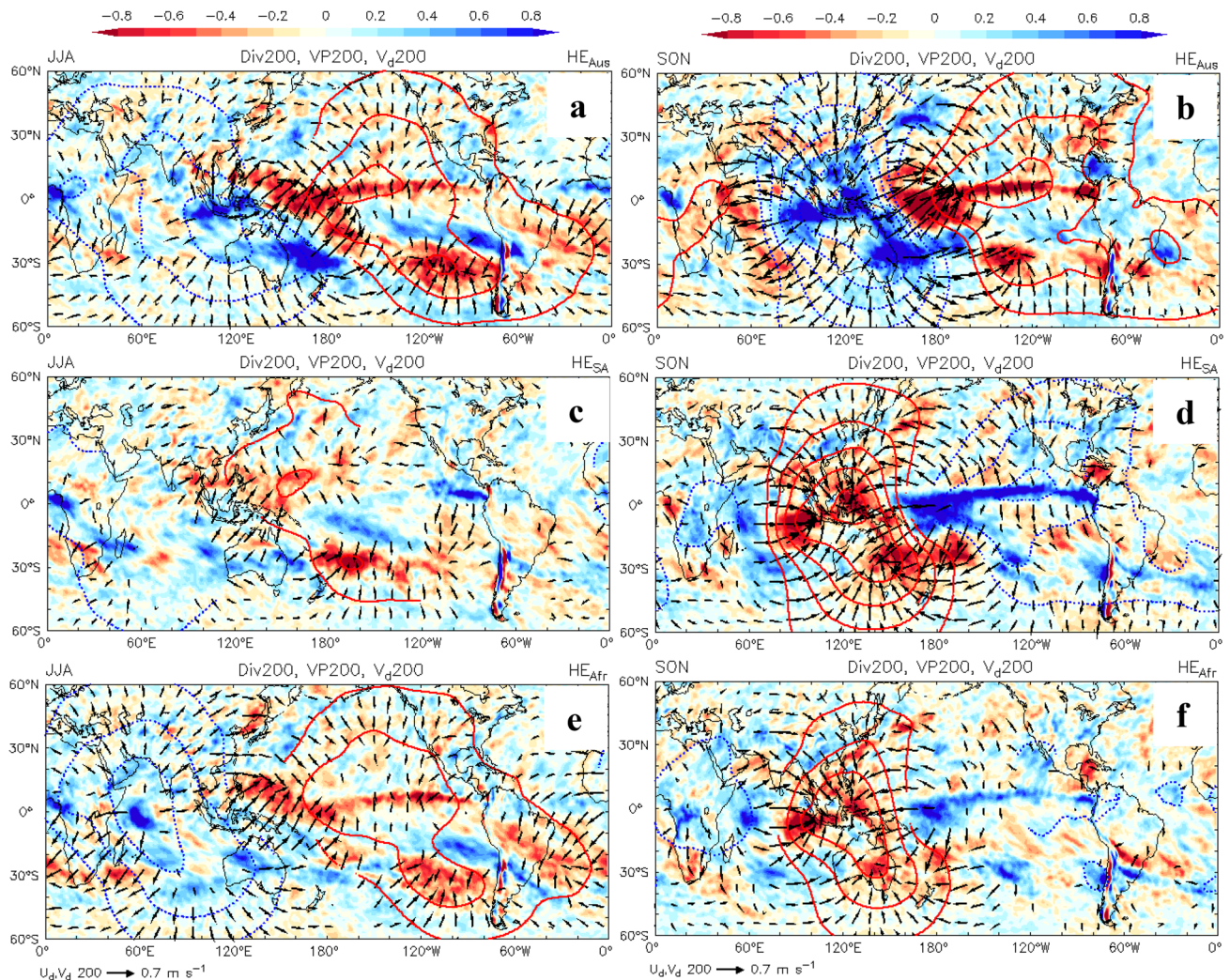


**Fig. 8** Same as Fig. 6 but for winter (*left*) and spring (*right*) and regressed onto standardized **a, b**  $HE_{Aus}$ , **c, d**  $HE_{SA}$  and **e, f**  $HE_{Afr}$

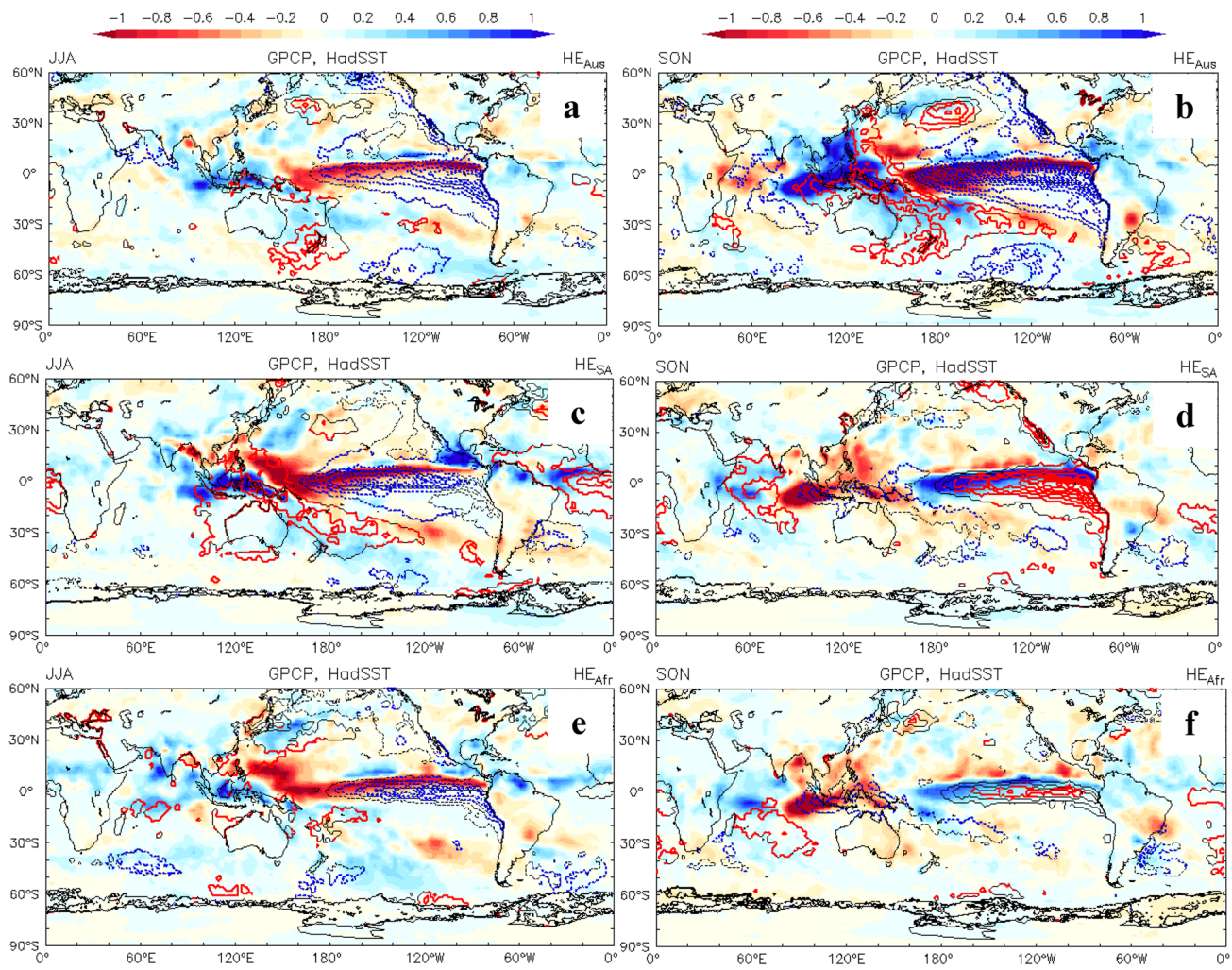


**Fig. 9** Same as Fig. 8 but the regressed variables are rainfall (shading) and SST (contour) anomalies

HE in the Australian sector in both winter and spring is associated with a positive swing in the Southern Oscillation, cyclonic anomalies over Australia and a PSA wave train radiating into the extratropics of the SH. In contrast, the circulation patterns associated with expanded HEs in the American and African sectors demonstrate a strong seasonality. During winter, a positive swing in the Southern Oscillation and a PSA wave train emanating from the tropical Pacific are also evident for HE<sub>SA</sub> and HE<sub>Afr</sub> although they are a little noisier. During spring, however, expansion of HE<sub>SA</sub> and HE<sub>Afr</sub> is associated with a negative phase of the Southern Oscillation (i.e. El Niño). Expansion of HE<sub>SA</sub> is further bolstered by the Rossby wave train emanating from the Indian Ocean associated with the positive IOD event that typically accompanies El Niño (e.g. Cai et al. 2011), while expansion of HE<sub>Afr</sub> is bolstered by increased rainfall over tropical Africa and Western Indian Ocean. Hence, expansion of HE<sub>SA</sub> and HE<sub>Afr</sub> during spring appears to result from both

local tropical forcing and remotely-forced extratropical changes.

In summer, the opposite relationships between the HEs are also observed similarly to spring (Fig. 4). However the regressed patterns differ from those onto spring (not shown). The main difference between summer and spring is that in summer the regression pattern is more dominated by the SAM and less of the IOD signature. This is because in summer the SAM is promoted by la Niña while IOD weakens.

## 6 Concluding remarks

This study extends the classical view of the zonal mean meridional circulation by exploring the variability of the HCs on a regional basis, specifically focusing on causes and nature of variations of HEs in the SH as determined by variations in location of the poleward edge of the sinking

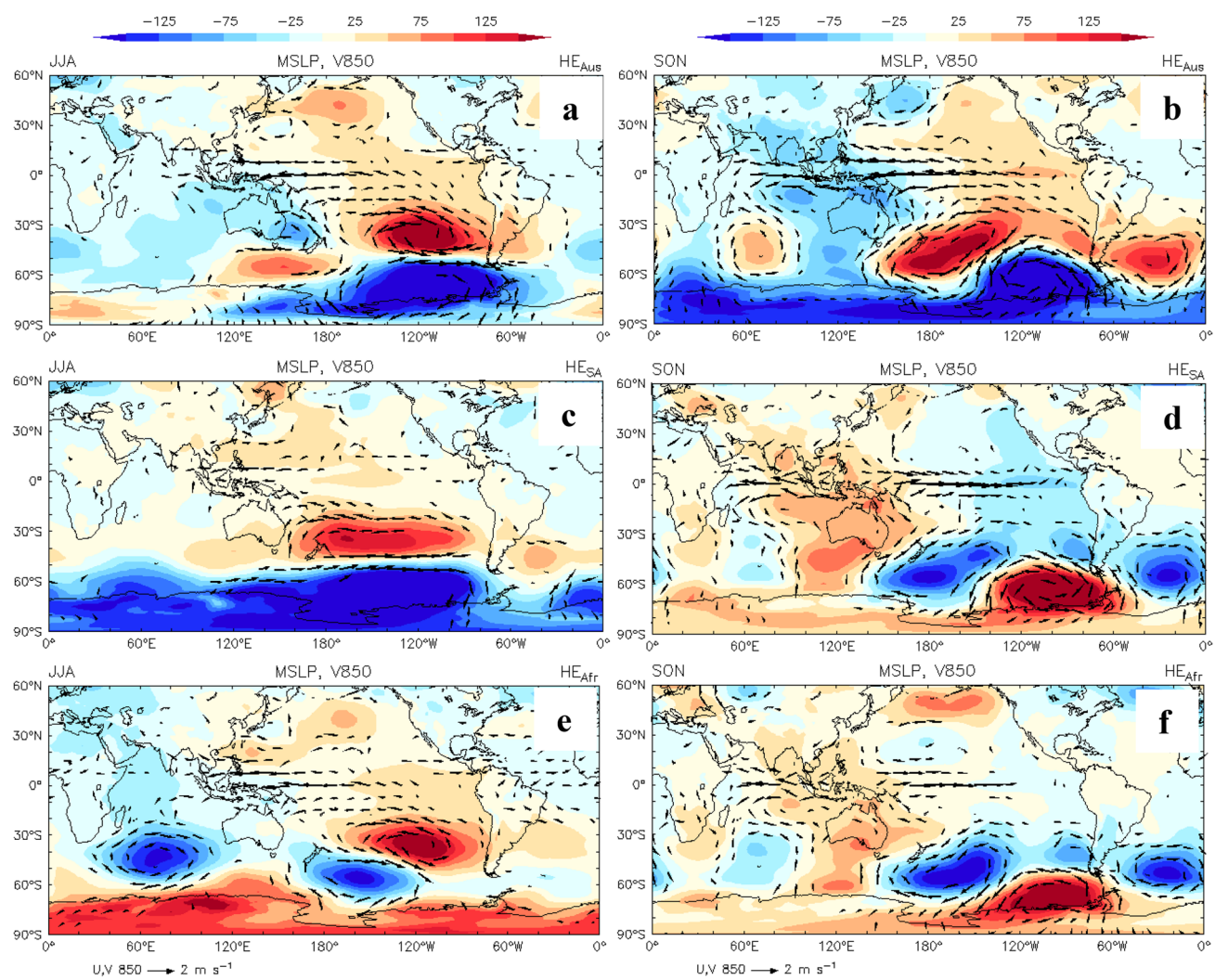


**Fig. 10** Same as Fig. 8 but the regressed variables are MSPL (shading) and 850 hPa wind (vector) anomalies

branch. Focusing on regional variations of the HEs highlights the interplay between the variability of the Walker (east–west) divergent and the meridional HC. By dividing the globe into three natural regions centered on the key heat sources over the Maritime Continent, South America and Africa, we highlighted how variations in each of these regions co-vary with each other and with the hemispheric mean cell. An important finding from this study is that the interannual variations of the zonal mean HE over the SH are dominated by what is happening in the Asia-Pacific sector, which is a direct response to variations of the largest tropical convective heat source located over Maritime Continent.

We further explored how the HC extent in each sector relates to ENSO, the IOD, and the SAM, especially focusing on the seasonality of these relationships. For ENSO, the strongest association is during austral spring and summer, when La Niña tends to promote an expanded hemispheric

and Australian sector cell but acts to contract the South American and African cells. During winter, all three cells tend to expand in conjunction with La Niña. We proposed that the opposing behavior of  $HE_{SA}$  and  $HE_{Afr}$  compared to the  $HE_{HS}$  and  $HE_{Aus}$  during spring/summer reflects the coupling of the regional HCs via the transverse Walker circulation: La Niña acts to intensify the Walker circulation in the Pacific, driving enhanced rainfall and divergence in the Australian sector and reducing rainfall and convergence in the South American and African sectors. The development of the IOD during spring in conjunction with ENSO further acts to enhance the opposite behavior of the African and South American sectors via changes in the Walker Circulation in the Indian Ocean and extratropical Rossby wave trains that influence the climate of subtropical Indian Ocean and South America.

We also highlighted that the high phase of the SAM is associated with both an expanded hemispheric (e.g. Kang

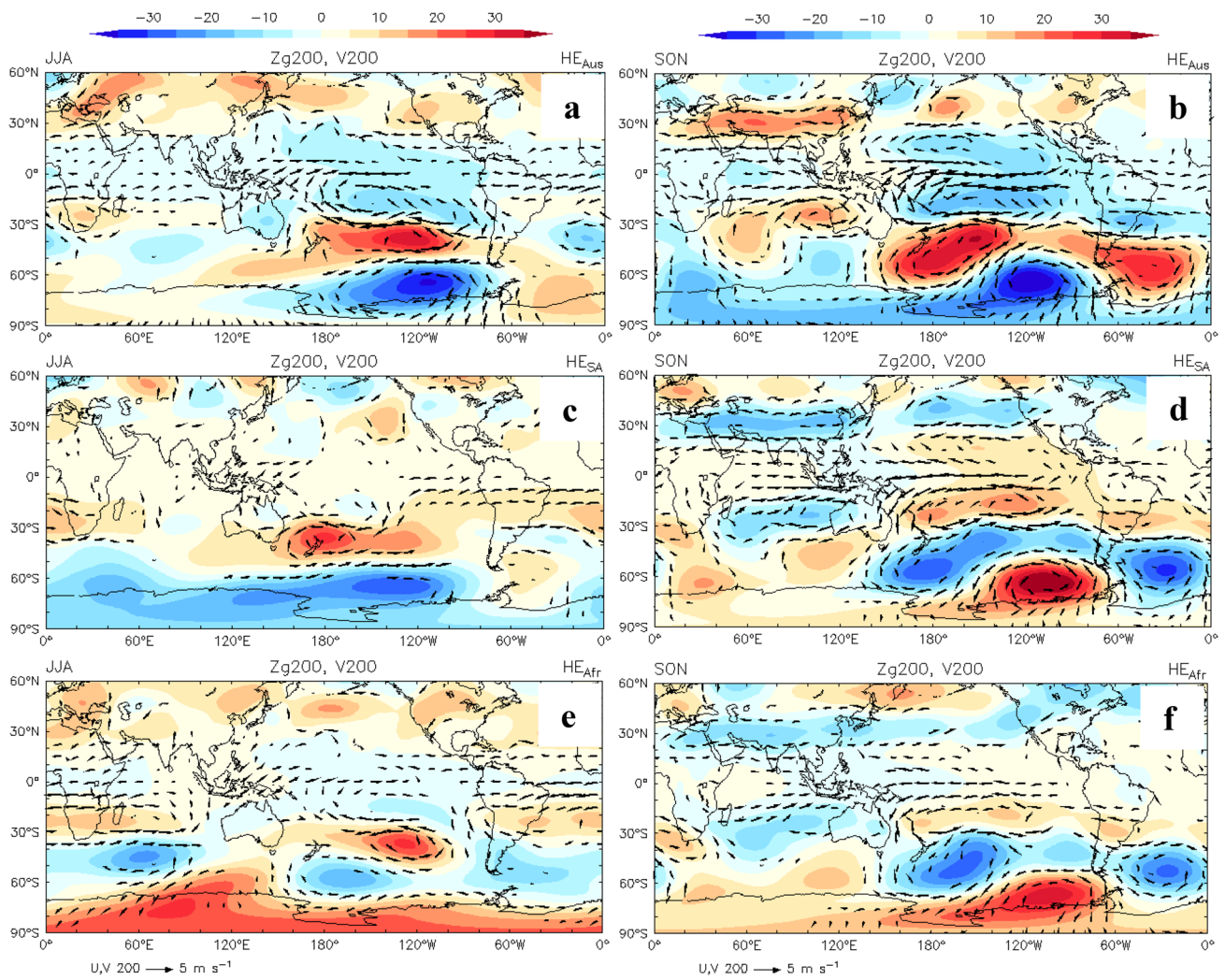


**Fig. 11** Same as Fig. 8 but the regressed variables are 200 hPa geopotential height (shading) and wind (vector) anomalies

and Polvani 2011) and Australian sector cell during spring/summer but not winter. A significant portion of this seasonality of the linkage between an expanded HC and high SAM is promoted by La Niña, which has been well established by earlier studies (Seager et al. 2003; L'Heureux and Thompson 2006; Lim et al. 2013; Lim and Hendon 2015). The absence of a relationship between the meridional extent of HC and SAM in austral winter was attributed by Hendon et al. (2014) to the presence of the strong wintertime subtropical jet, which plays a buffering role between the tropics and the SH extratropics.

Tropical SST variability associated with ENSO was identified as the key mechanism driving variability of the Southern Hemisphere HC. La Niña conditions drive an expansion in the Australian sector in excess of the hemispheric mean due to compensating contraction in the Africa and South America sectors. This offers a plausible hypothesis to explain climate models' underestimate of

the observed tropical expansion during the last 50 years (Nguyen et al. 2015). That is, part of the recent expansion presumably would have been driven by a swing from warm to cold phase of the Interdecadal Pacific Oscillation (IPO) conditions during the last 30 years (e.g., Meehl et al. 2016), which is akin to a swing toward a La Niña-like conditions. This swing to the cold phase of the IPO anomalies is not captured in the ensemble mean of historical simulations (e.g., Johanson and Fu 2009; Quan et al. 2014). However, if that swing from warm to cold IPO was the sole explanation of the observed expansion in the Southern Hemisphere, then one would expect to have observed a contraction in the African and South American sectors. However, this is not consistent with the observed regional tropical expansion deduced from radiosonde data (Lucas et al. 2012), and therefore, other factors could be contributing to the expansion, especially external anthropogenic forcings (e.g., Nguyen et al. 2015).

Our future work will focus on understanding how much of the observed recent trends in HEs can be accounted for by observed trends in key modes of climate variability including the IPO, the IOD, ENSO and the SAM. We will also examine the capability of climate models to simulate the variability and trends of regional HEs associated with those of the key climate modes, which may, in turn, shed some light on the uncertainty of future projections of HC extent.

**Acknowledgements** This project is supported by the Victorian Climate Initiative (VicCI). E. Maloney was supported by the Climate and Large-Scale Dynamics Program of the National Science Foundation under Grant AGS-1441916, and G. Boschat by the Australian Research Council grant DP140102855. We warmly thank Josephine Brown and Kevin Tory for their insightful comments on the manuscript prior to submission.

## References

- Ashok K, Behera SK, Rao SA, Weng H, Yamagata T (2007) El Niño Modoki and its possible teleconnection. *J Geophys Res* 112:C11007. doi:[10.1029/2006JC003798](https://doi.org/10.1029/2006JC003798)
- Birner T, Davis SM, Seidel DJ (2014) The changing width of Earth's tropical belt. *Phys Today* 12:38–44
- Butle AH, Thompson DW, Birner T (2011) Isentropic slopes, downgradient eddy fluxes, and the extratropical atmospheric circulation response to tropical tropospheric heating. *J Atmos Sci* 68(10):2292
- Cai W, van Rensch P, Cowan T, Hendon HH (2011) An asymmetry in the IOD and ENSO teleconnection pathway and its impact on Australian climate. *J Clim* 25:6318–6329
- Chen G, Held IM (2007) Phase speed spectra and the recent poleward shift of Southern Hemisphere surface westerlies. *Geophys Res Lett* 34:L21805. doi:[10.1029/2007GL031200](https://doi.org/10.1029/2007GL031200)
- Chen S, Wei K, Chen W, Song L (2014) Regional changes in the annual mean Hadley circulation in recent decades. *J Geophys Res* 119. doi:[10.1002/2014JD021540](https://doi.org/10.1002/2014JD021540)
- Davis SM, Rosenlof KH (2012) A multi-diagnostic intercomparison of tropical width time series using reanalyses and satellite observations. *J Clim* 25:1061–1078. doi:[10.1175/JCLI-D-11-00127.1](https://doi.org/10.1175/JCLI-D-11-00127.1)
- Dee DP, Uppala SM, Simmons AJ, Berrisford P, Poli P, Kobayashi S, Andrae U, Balmaseda MA, Balsamo G, Bauer P et al (2011) The ERA-Interim reanalysis: configuration and performance of the data assimilation system. *Q J R Meteorol Soc* 137:553–597. doi:[10.1002/qj.828](https://doi.org/10.1002/qj.828)
- Fyfe JC, Boer GJ, Flato GM (1999) The arctic and antarctic oscillations and their projected changes under global warming. *Geophys Res Lett* 26:1601–1604. doi:[10.1029/1999GL900317](https://doi.org/10.1029/1999GL900317)
- Gill AE (1980) Some simple solutions for heat induced tropical circulation. *Quart J Roy Meteor Soc* 106:447–462
- Gillett NP, Fyfe JC (2013) Annular mode changes in the CMIP5 simulations. *Geophys Res Lett* 40:1189–1193. doi:[10.1002/grl.50249](https://doi.org/10.1002/grl.50249)
- Hendon HH, Thompson DWJ, Wheeler MC (2007) Australian rainfall and temperature variations associated with the Southern Hemisphere Annular Mode. *J Clim* 20:2452–2467
- Hendon HH, Lim E-P, Nguyen H (2014) Seasonal variations of subtropical precipitation associated with the southern annular mode. *J Clim* 27:3446–3460. doi:[10.1175/JCLI-D-13-00550.1](https://doi.org/10.1175/JCLI-D-13-00550.1)
- Hu Y, Zhou C, Liu J (2011) Observational evidence for the poleward expansion of the Hadley circulation. *Adv Atmos Sci* 28:33–44. doi:[10.1007/s00376-010-0032-1](https://doi.org/10.1007/s00376-010-0032-1)
- Huffman GJ, Adler RF, Bolvin DT, Gu G (2009) Improving the global precipitation record: GPCC version 2.1. *Geophys Res Lett* 36:L17808. doi:[10.1029/2009GL040000](https://doi.org/10.1029/2009GL040000)
- Johanson CM, Fu Q (2009) Hadley cell widening: model simulations versus observations. *J Clim* 22:2713–2725. doi:[10.1175/2008JCLI2620.1](https://doi.org/10.1175/2008JCLI2620.1)
- Kang SM, Polvani LM (2011) The interannual relationship between the latitude of the eddy-driven jet and the edge of the hadley cell. *J Clim* 24:563–568. doi:[10.1175/2010JCLI4077.1](https://doi.org/10.1175/2010JCLI4077.1)
- Kang SM, Polvani LM, Fyfe JC, Son S-W, Sigmund M, Correa GJP (2013) Modeling evidence that ozone depletion has impacted extreme precipitation in the austral summer. *Geophys Res Lett* 40:4054–4059. doi:[10.1002/grl.50769](https://doi.org/10.1002/grl.50769)
- Kao H-Y, Yu J-Y (2009) Contrasting eastern-Pacific and central-Pacific types of ENSO. *J Clim* 22:615–632. doi:[10.1175/2008JCLI2309.1](https://doi.org/10.1175/2008JCLI2309.1)
- L'Heureux ML, Thompson DWJ (2006) Observed relationships between the El Niño–Southern Oscillation and the extratropical zonal-mean circulation. *J Clim* 19:276–287. doi:[10.1175/JCLI3617.1](https://doi.org/10.1175/JCLI3617.1)
- Lim E-P, Hendon HH (2015) Understanding and predicting the strong Southern Annular Mode and its impact on the record wet east Australian spring 2010. *Clim Dyn* 44:2807–2824
- Lim E-P, Simmonds I (2009) Effect of tropospheric temperature change on the zonal mean circulation and SH winter extratropical cyclones. *Clim Dyn* 33:19–32
- Lim E-P, Hendon HH, Rashid HA (2013) Seasonal predictability of the Southern Annular Mode due to its association with ENSO. *J Clim* 26:8037–8054
- Lim E-P, Hendon HH, Arblaster JM, Delage F, Nguyen H, Min S-K, Wheeler MC (2016) The impact of the Southern Annular Mode on future changes in Southern Hemisphere rainfall. *Geophys Res Lett* 43:7160–7167. doi:[10.1002/2016GL069453](https://doi.org/10.1002/2016GL069453)
- Lu J, Chen G, Frierson DMW (2008) Response of the zonal mean atmospheric circulation to El Nino versus global warming. *J Clim* 21:5836–5851
- Lucas C, Nguyen H (2015) Regional characteristics of tropical expansion and the role of climate variability. *J Geophys Res Atmos* 120. doi:[10.1002/2015JD023130](https://doi.org/10.1002/2015JD023130)
- Lucas C, Nguyen H, Timbal B (2012) An observational analysis of Southern Hemisphere tropical expansion. *J Geophys Res* 117:D17112. doi:[10.1029/2011jd017033](https://doi.org/10.1029/2011jd017033)
- Lucas C, Timbal B, Nguyen H (2013) The expanding tropics: a critical assessment of the observational and modelling studies. *WIREs Clim Change* doi:[10.1002/wcc.251](https://doi.org/10.1002/wcc.251)
- Meehl GA, Santer BD, Xie S-P (2016) Contribution of the Interdecadal Pacific Oscillation to twentieth-century global surface temperature trends. *Nat Clim Change* 6:1005–1008. doi:[10.1038/nclimate3107](https://doi.org/10.1038/nclimate3107)
- Miller RL, Schmidt GA, Shindell DT (2006) Forced annular variations in the 20th century Intergovernmental Panel on Climate Change Fourth Assessment Report models. *J Geophys Res* 111:D18101. doi:[10.1029/2005JD006323](https://doi.org/10.1029/2005JD006323)
- Moore GWK, Alverson K, Holdsworth G (2004) Mount logan ice core evidence for changes in the hadley and walker circulations following the end of the little ice age. Chapter 13, The hadley circulation: present, past and future, ed. Diaz and Bradley, Kluwer Academic Publisher, pp. 371–395
- Nguyen H, Evans A, Lucas C, Smith I, Timbal B (2013) The hadley circulation in reanalyses: climatology, variability and expansion. *J Clim* 26:3357–3376. doi:[10.1175/JCLI-D-12-00224](https://doi.org/10.1175/JCLI-D-12-00224)
- Nguyen H, Lucas C, Evans A, Timbal B, Hanson L (2015) Expansion of the Southern Hemisphere Hadley Cell in response to

- greenhouse gas forcing. *J Clim* 28:8067–8077. doi:[10.1175/JCLI-D-15-0139.1](https://doi.org/10.1175/JCLI-D-15-0139.1)
- Oort AH, Yienger JJ (1996) Observed interannual variability in the Hadley circulation and its connection to ENSO. *J Climate* 9:2751–2767
- Purich A, Cowan T, Min S-K, Cai W (2013) Autumn precipitation trends over Southern Hemisphere midlatitudes as simulated by CMIP5 models. *J Clim* 26(21):8341–8356. doi:[10.1175/JCLI-D-13-00007.1](https://doi.org/10.1175/JCLI-D-13-00007.1)
- Quan X, Hoerling M, Perlitz J, Diaz H, Xu T (2014) How fast Are the tropics expanding? *J Clim* 27:1999–2013. doi:[10.1175/JCLI-D-13-00287.1](https://doi.org/10.1175/JCLI-D-13-00287.1)
- Rayner NA, Parker DE, Horton EB, Folland CK, Alexander LV, Rowell DP, Kent EC, Kaplan A (2003) Global analyses of sea surface temperature, sea ice, and night marine air temperature since the late nineteenth century. *J Geophys Res* 108(D14):4407. doi:[10.1029/2002JD002670](https://doi.org/10.1029/2002JD002670)
- Saji NH, Goswami BN, Vinayachandran PN, Yamagata T (1999) A dipole mode in the tropical Indian Ocean. *Nature* 401:360–363
- Schwendike J, Govekar P, Reeder MJ, Wardle R, Berry GJ, Jakob C (2014) Local partitioning of the overturning circulation in the tropics and the connection to the Hadley and Walker circulations. *J Geophys Res Atmos* 119(3):1322–1339. doi:[10.1002/2013JD020742](https://doi.org/10.1002/2013JD020742)
- Schwendike J, Berry GJ, Reeder MJ, Jakob C, Govekar P, Wardle R (2015) Trends in the local Hadley and local Walker circulations. *J Geophys Res Atmos* 120:7599–7618. doi:[10.1002/2014JD022652](https://doi.org/10.1002/2014JD022652)
- Seager R, Harnik N, Kushnir Y, Robinson W, Miller J (2003) Mechanisms of hemispherically symmetric climate variability. *J Clim* 16:2960–2978. doi:[10.1175/1520-0442\(2003\)016<2960:MOHS>2.0.CO;2](https://doi.org/10.1175/1520-0442(2003)016<2960:MOHS>2.0.CO;2)
- Seidel DJ, Fu Q, Randel WJ, Reichler TJ (2008) Widening of the tropical belt in a changing climate. *Nat Geosci* 1:21–24. doi:[10.1038/ngeo.2007.38](https://doi.org/10.1038/ngeo.2007.38)
- Son S-W, Polvani LM, Waugh DW, Akiyoshi H, Garcia RR, Kinnison D, Pawson S, Rozanov E, Shepherd TG, Shibata K (2008) The impact of stratospheric ozone recovery on the Southern Hemisphere westerly jet. *Science* 320:1486–1489
- Staten PW, Rutz JJ, Reichler T, Lu J (2011) Breaking down the tropospheric circulation response by forcing. *Clim Dyn* 39:2361–2375. doi:[10.1007/s00382-011-1267-y](https://doi.org/10.1007/s00382-011-1267-y)
- Taschetto AS, England MH (2009) El Niño Modoki impacts on Australian rainfall. *J Clim* 22:3167–3174. doi:[10.1175/2008JCLI2589.1](https://doi.org/10.1175/2008JCLI2589.1)
- Thompson DWJ, Wallace JM (2000) Annular modes in the extratropical circulation. Part I: month-to-month variability. *J Clim* 13:1000–1016
- Yin JH (2005) A consistent poleward shift of the storm tracks in simulations of 21st century climate. *Geophys Res Lett* 32:L18701. doi:[10.1029/2005GL023684](https://doi.org/10.1029/2005GL023684)
- Zhao M, Hendon HH (2009) Representation and prediction of the Indian Ocean dipole in the POAMA seasonal forecast model. *QJR Meteorol Soc* 135:337–352. doi:[10.1002/qj.370](https://doi.org/10.1002/qj.370)
- Zheng F, Li J, Clark RT, Nnamchi HC (2014) Simulation and projection of the Southern Hemisphere annular mode in CMIP5 models. *J Clim* 26:9860–9879